LASER EMISSION AND AUTODYNE SPECTROSCOPY OF THE ATMOSPHERE AND UNDERLYING SURFACE

Yu.D. Kopytin

Institute of Atmospheric Optics,
Siberian Branch of the Russian Academy of Sciences, Tomsk
Received January 21, 1997

A review is presented of the methods for laser sensing of the atmospheric parameters developed by the author. The results of investigations are given on problems of self-action of high-power laser beams propagating in the surface layer of the outdoor atmosphere which comprises aerosol particles. Possible applications of an aerosol spectrochemical (ASC) lidar to an elemental emission analysis of aerosol substance in a remote laser spark and opto-acoustic sensing of the meteorological parameters are studied. Most attention is concentrated on a novel class of lidar systems, namely, laser reception (LR) lidars which provide the record spectral sensitivity of path gas analysis and detection of acoustic and microcapillary waves.

INTRODUCTION

The advancement of high-power laser technique opens up new possibilities for application of the specific and very wide class of processes of nonlinear coherent light interaction with a medium as a physical basis for novel methods of laser sensing of the atmospheric parameters, first of all, that cannot be measured by conventional linear optics methods.

The present paper systematizes the main results of investigations into the above-indicated problem obtained with my participation. Investigations on the problem of self-action of high-power laser pulses propagating in the surface layer of the outdoor atmosphere which comprises aerosol particles allow us to formulate and to implement the idea of an aerosol spectrochemical (ASC) lidar for elemental emission analysis of aerosol substance in a remote laser spark and opto-acoustic measurements of the meteorological parameters.

A large part of this paper is concerned with the results of investigations of a novel class of lidar systems, namely, laser reception (LR) lidars, which provide the record spectral sensitivity of path gas analysis and detection of acoustic and microcapillary waves. Highly nonlinear selective response of a laser autodyne to external optical signals is used as a useful physical phenomenon in the LR lidars.

1. SPECTROCHEMICAL AND OPTO-ACOUSTIC MEASUREMENTS IN A LASER SPARK

1.1. ASC lidars

The aerosol spectrochemical lidar is based on an analysis of remote laser-induced atomic emission spectra of aerosol particles. It is highly selective.[1-5] When a high-power laser beam is focused into the atmosphere, aerosol particles are heated to high temperatures upon exposure to this beam and are evaporated. This process is accompanied by the cascade ionization evolving in vapors surrounding the particles. Atoms and molecules of vapors are excited in the process of inelastic collisions with free high-temperature plasma electrons.

The energy emitted from breakdown regions formed in vapor-gas halos surrounding aerosol particles is manifested through a set of spectral lines, recombination continuum, and thermal radiation of particles heated by laser radiation. Theoretical calculation of the emission spectra is a complex problem due to a wide variety of aerosol chemical compositions and nonequilibrium levels of excitation in plasma of the pulsed optical breakdown. In this connection, the emphasis is on experimental investigations in model aerosol media and the outdoor atmosphere.[2-9]

The laser threshold power density I_{th} required to initiate the optical breakdown was determined in Refs. 2–4 and 9 as a function of the size and number density of aerosol particles. The most efficient source of radiation for spectrochemical atmospheric applications is a pulsed CO_2 laser at $\lambda = 10.6$ μm, because the majority of condensed substances have strong absorption bands in this spectral region and the efficiency of cascade ionization in vapors, proportional to λ^2, is high.

The optical emission spectrum of a substance induced by laser pulses with duration <1 μs is electroluminescent by its nature due to a higher temperature of free electrons in comparison with atoms and molecules of the medium. This increases significantly the signal-to-noise ratio as compared with emission spectroscopy of equilibrium arc discharge.

Our experiments also show that for coarsely dispersed particles of different chemical compositions with sizes greater than 3 μm the breakdown threshold power density of laser radiation is practically independent of the particle sizes ($I_{th} = (1–3) \cdot 10^7$ W/cm² at λ = 10.6 μm). For submicron particles the threshold power density of laser radiation increases monotonically and approaches the clear air breakdown threshold ($I_{th} = (2–3) \cdot 10^9$ W/cm² at λ = 10.6 μm). For large number densities of coarsely dispersed aerosols the breakdown threshold decreases by about an order of magnitude because of cooperative low-threshold mechanism of optical breakdown ($I_{th} = 2 \cdot 10^6$ W/cm² at λ = 10.6 μm). It should be pointed out that currently achieved energy parameters of lasers of other types, in particular, Nd-glass and HF lasers, allow their application to remote initiation of plasma formations by aerosol particles as well.

The low-threshold breakdown initiated by aerosol particles in the atmosphere is random in character due to the random probability of turbulent overshoots of the laser radiation intensity I (its speckle structure) on the one hand, and on the other hand, the Poisson statistics of the event that the aerosol particle with the size exceeding the critical one $a \geq a_{cr}(I)$ enters the caustic of the focused laser beam.

The following equation is valid for the total probability of plasma formations with the number density N_{pf}:

$$p(N_{th}) = (N_{th}!)^{-1} \left[\left\langle \int_{a_{cr}}^{\infty} n_0(a)\, da \right\rangle_I \right]^{N_{th}} \exp\left[- \left\langle \int_{a_{cr}}^{\infty} n_0(a)\, da \right\rangle_I \right],$$

where the angular brackets of the form $\langle\ \rangle_I$ denote averaging over all possible spatial realizations of the laser beam intensity I, $n_0(a)$ is the size distribution function of aerosol particles, in cm⁻³. The results of numerical modeling of plasma formation statistics in the atmosphere with the lognormal distribution of the CO_2-laser radiation intensity (λ = 10.6 μm) are presented in Ref. 1.

In the mobile ASC lidar[3,4,9] developed at the IAO SB RAS the emission spectrum of aerosols is induced by an electroionization CO_2 laser with maximum output energy of 500 J per pulse, a pulse duration of 300 ns at half maximum of the main peak and gradually falling trailing edge of the pulse 1.5 μs long. A laser beam is formed by a Cassegrain reflecting telescopic system with a large parabolic mirror 500 mm in diameter and a small hyperbolic mirror 110 mm in diameter. The focal distance that specifies the sensing range is changed from 50 to 250 m by the displacement of a counter reflector. Scanning over elevation angles is performed

by the rotation of the telescope around the horizontal axis. The telescope detects simultaneously the radiation emitted by plasma formations. This automatically provides matching of receiving and transmitting lidar channels. Laser and plasma light fluxes are split with a plate fabricated from BaF_2, which transmits the radiation at λ = 10.6 μm and reflects the visible plasma radiation at the angle of total internal reflection. A system of spectral recording of the plasma radiation comprises a focusing lens, a diffraction spectrometer, a TV camera with a built-in amplifier on microchannel plates, and a display interfaced with an IBM PC. The ASC lidar has the following specifications: sensing range up to 250 m, spatial resolution 3–6 m, average sensitivity to mass concentration 0.1–10.0 μg/m³, average relative error of 30%, and the number of simultaneously measured elements up to 50. In analogy with Ref. 33, to optimize the ratio of the signal to the background continuum, we used temporal strobing of the pulsed spectrum with 5–10 μs strobes.

Incorporation of an acoustic channel into the spectrochemical lidar allows us to determine simultaneously the distance to the breakdown region and the number density of plasma formations.

An important advantage of the method for direct spectral analysis of elements based on their emission spectra is its high sensitivity to small concentrations of examined elements[3,7,8,11–14] which allows us to monitor mass concentrations of highly toxic and radioactive elements. Figure 1 shows the mass concentration of beryllium in aerosols inside a facility when the optical air breakdown was induced by the pulsed CO_2-laser radiation.[7] The vertical solid line indicates the maximum permissible mass concentration of beryllium inside a facility. An advantage of CO_2 laser over the Nd-glass laser can be clearly seen in the region of ultimately low mass concentrations. The figure illustrates the feasibility of reliable detection of ultimately low concentrations of beryllium.
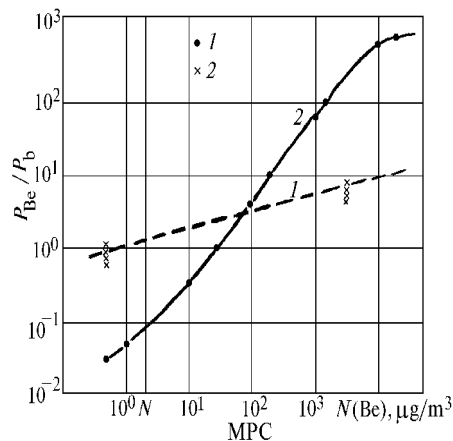

FIG. 1. Measurements of the beryllium mass concentration in aerosols inside a facility when the optical air breakdown was induced by pulsed CO_2 (1) and Nd-glass (2) lasers. Here, P_{Be}/P_b is the ratio of the signal power to the background noise power.

Figure 2 illustrates the spectrum of the UO_2F_2 (uranyl fluoride) particles that initiated plasma formations upon exposure to pulses of CO_2-laser radiation[8] with a pulse duration of 1.5 μs. Detection was performed against the spectral line of uranium ion at λ = 409.013 nm.

Practically complete absence of the background noise calls our attention. This allows us to identify even weak lines of the uranium spectrum. In the course of the experiments with uranyl fluoride dissolved in distilled water the droplet sizes were varied from 100 μm to 1 mm. The concentration of uranium atoms in the breakdown region was less than 2 ppm. The sensitivity achieved in the experiments on uranium detection in solid particles was twice as high as the maximum sensitivity reported in Ref. 14. In conclusion, it should be mentioned that the method and instrumentation described above can be used for an express analysis of elemental composition of the underlying surface.
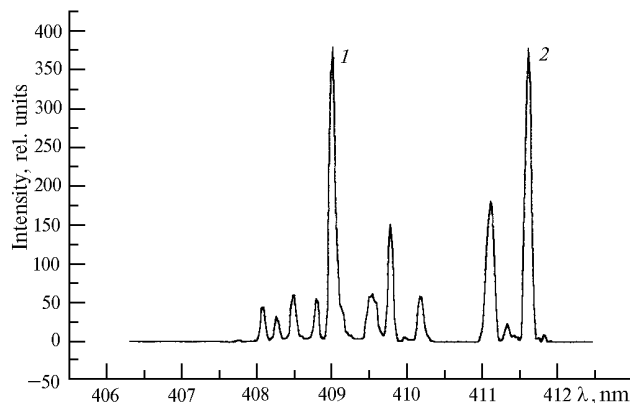

FIG. 2. Spectrum obtained by processing of a recorded image. The time delay is 4.2 μs. Numbers 1 and 2 designate the lines of uranium ion at λ = 409.013 and 411.610 nm, respectively.

1.2. Opto-acoustic methods for sensing of the surface atmospheric layer

The acoustic radiation generated by the laser breakdown in the atmosphere is of special interest for the problem of sensing, because it bears information on the laser radiation and gas-disperse medium which absorbs this radiation. In addition, artificial source of acoustic radiation induced by the laser radiation can be used in conventional schemes of acoustic sounding, for instance, to determine spectral acoustical and meteorological parameters in the lower 1-km layer of the atmosphere.[15-18]

A discrete laser spark in the atmosphere generates optical and high-power broadband acoustic radiation. The latter is a superposition of hydrodynamic perturbations from individual plasma formations. The sound pressure level reaches 100−150 dB at a distance of 1.5 m from the laser spark.

Acoustic effects accompanying the laser breakdown in the outdoor atmosphere were studied as part of the integrated experiment described in Refs. 15 and 16. The maxima in the acoustic spectra were observed mainly in the octave band centered at 4 kHz. Spectral wings decayed with a rate of 6 dB per octave, in analogy with a point explosion. Reflections of the sound wave from the underlying surface make the acoustic signal processing difficult and should be taken into account in experimental design and performance in the surface atmospheric layer.

The method for reconstruction of the critical size of the particle initiating macrobreakdown a_{cr} from acoustic measurements was developed in Ref. 15. It is based on solving the equation

$$\int_{a_{cr}}^{\infty} n_0(a) \, da = \langle N_{pf}(W) \rangle,$$

where $n_0(a)$ is the initial particle size distribution function, $\langle N_{pf}(W) \rangle$ is the number density of plasma formations averaged over random realizations, which depends on the laser pulse energy density W.

A number of methods for remote determination of the atmospheric parameters including the temperature, the wind velocity vector, the humidity, and the spectral acoustic transparency harnessing opto-acoustic phenomena in the laser spark are suggested in Refs. 16–18. The essence of these methods is as follows. An opto-acoustic laser radar measures in real time the frequency spectra of acoustic signals and the time delay between acoustic signal and light plasma pulse arrival at different acoustic frequencies for a set of altitudes and different arrangements of the acoustic source and antennas. Then the desired parameters are determined with the use of known analytical or tabular relations between the measurable and atmospheric parameters.

2. LR LIDARS FOR ATMOSPHERIC GAS ANALYSIS AND AUTODYNE MEASUREMENTS IN OPTICAL DETECTION AND RANGING

2. 1. Autodyne method of echo-signal reception on a laser

Laser reception lidars (LR lidars) harness the physical effect of nonlinear response of a laser as a self-oscillating circuit (autodyne) to a weak external optical signal.[1,19-22]

The laser radiation scattered by an external mirror or a topographic object is selectively absorbed on the atmospheric path and received by the laser. In the laser cavity, it interacts with the reference radiation. If the duration of the external signal exceeds the characteristic photon lifetime in the laser cavity t_{ph}, nonlinear redistribution of the laser power, generated at competitive transitions and modes, is possible. Owing

to the similarity of physical processes in the cavity with active element, the LR-lidar methods have the spectral sensitivity comparable with the method of intracavity laser spectroscopy[23,24] (ICLS). These methods differ as follows. In the case of ICLS, weak frequency-dependent losses (a cell with an absorbing gas) are inserted into the laser cavity, while in the LR-lidar method, a weak frequency-dependent external signal enters the cavity. Efficiency of the autodyne echo-signal reception schemes, as in the case of conventional (off-cavity) heterodyne reception, increases with the laser temporal coherence.

Interest in the autodyne reception on the laser has noticeably quickened in the last few years.[25-28] This is connected with the possibility of significant gain in spectral sensitivity (by several orders of magnitude) of absorption laser gas analysis in case of remote detection of ultimately low concentrations of gas pollutants and vapors of highly toxic, narcotic, explosive, and other substances. In addition, the laser reception significantly improves the sensitivity and reduces noise in optical heterodyning of coherent echo signals, which enlarges the class of problems on optical detection and ranging, Doppler measuring, and vibrometry that can be solved by this method.

Specific requirements to the active element pumping level and the laser cavity parameters can be determined based on a theoretical analysis of broadband laser response to a frequency-dependent external action.

Let $u_{\pm}(\omega, z, t)$ be the complex amplitudes of the electric vector of optical fields propagating along the z axis in opposite directions inside the laser cavity with length l.

Let us introduce the designation $\sqrt{\langle u_{\pm} u_{\pm}^* \rangle} = S$. Then in the simplest case, the operation of a linear laser with a cavity formed by two mirrors with the power reflection coefficients r_1 and r_2, respectively, spaced along the z axis is described by the following boundary problem:

$$(\pm \, \partial/\partial z + v^{-1} \, \partial/\partial t) \, S_{\pm} = (k - \beta) \, S_{\pm} + j_{\pm} \, , \qquad (1)$$

$$S_{+}(\omega, 0, t) = r_1 \, S_{-}(\omega, 0, t), \qquad (2)$$

$$S_{-}(\omega, l, t) \approx r_2 \, \{ S_{+}(\omega, l, t) +$$

$$+ \, \mu_n \, r_{\text{eff}} \, S_{+}(\omega, l, t - 2z/c) + \mu_c \, \bar{B}_c(t) \, (r_{\text{eff}}/r_2)^{1/2} \times$$

$$\times \, [S_{+}(\omega, l, t) \, S_{+}(\omega, l, t - 2z/c)]^{1/2} \} \, , \qquad (3)$$

where v and c are the light velocities in the laser active medium and the atmosphere, respectively; $k(\omega)$ and β are the coefficients of spectral amplification and nonselective losses in the active medium; $j_{\pm}$ is the power of spontaneous relaxation of excited centers of the active medium; ω is the radiation frequency; t is time; $\bar{B}_c(t)$ is the coefficient of temporal correlation of the reference and reflected fields in the image plane of the receiving telescope averaged over the image

aperture; coefficients μ_n and μ_c consider the peculiarities of echo-signal reception. For completely coherent reception, $\mu_n = 0$ and $\mu_c = 1$. In the opposite case, $\mu_n = 1$ and $\mu_c = 0$. The effective coefficient of external laser radiation reflection r_{eff} from the mirror or topographic object with albedo r_3 is defined as a ratio of returned radiation power and the emitted power considering the transmittance of the output mirror $(1 - r_2)$

$$r_{\text{eff}} = \left(\frac{R_0}{2z} \right)^2 \left(\frac{4}{\pi d_1^2} \right) (1 - r_2)^2 \frac{r_3}{r_2} \exp \left[-2 \int\limits_0^z \alpha_{\Sigma}(\omega, z') \, dz' \right], (4)$$

where d_1 is the diameter of the laser active element, R_0 is the aperture radius of the receiving telescope, $\alpha_{\Sigma}(\omega, z) = \alpha_g(\omega, z) + \alpha_e(z)$ is the volume absorption coefficient of the atmospheric aerosol and gas $[\text{cm}^{-1}]$ including selective (α_g) and nonselective (as compared with the laser gain bandwidth) absorption coefficients of gas and aerosol.

In its turn, the amplification coefficient $k(\omega)$ appearing in Eq. (1) is described either by a system of balance equations for population kinetics of coupled levels of laser transitions (for low-pressure gas lasers) or by the integro-differential equation for the number density of excited particles per unit of length for nonuniformly (uniformly) broadened gain line shape of solid-state (liquid) lasers.

To analyze signals recorded by a quadratic photodetector, it is expedient to manipulate with the root-mean-square photocurrent $\langle i^2 \rangle^{1/2}$ determined by the root-mean-square radiation intensity (radiant flux density) inside the laser cavity of length l:

$$I = l^{-1} \int\limits_0^l (S_{-} + S_{+}) \, dz.$$

Generally, the boundary problem expressed by Eqs.(1)−(3) with the equation for the laser amplification coefficient $k(\omega)$ and expression for the temporal coherence function $\bar{B}_c(t)$ of the scattered radiation is very cumbersome.[5,19,21] Therefore, below we restrict our consideration to a qualitative analysis of specific asymptotic cases which satisfy the following inequalities:

$$\eta_3 \geq 1, \quad \eta_3(\Delta t_2/\Delta t_1) \gg 1 \, , \qquad (5)$$

$$\eta_3 \ll 1, \quad \eta_3(\Delta t_2/\Delta t_1) \geq 1 \, , \qquad (6)$$

$$\eta_3 \ll 1, \quad \eta_3(\Delta t_2/\Delta t_1) \ll 1 \, , \qquad (7)$$

$$\eta_3 = \mu_n \, r_{\text{eff}} + \mu_c \, (2r_{\text{eff}}/r_2)^{1/2} \, \bar{B}_c(t) \, . \qquad (8)$$

a) In the first two cases described by inequalities (5)−(6), the external echo-signal affects highly nonlinearly the reference laser generation regime. In practice, this leads to self-locking of laser

frequency by the external signal, breakdown of laser generation, elongation of spikes, and a decrease in the frequencies of relaxation oscillations. At the same time, the laser parameters including spectral sensitivity can be controlled through variations of the parameter of external signal η_3, for instance, through variations of the reflectance r_2 of the laser output mirror. The effects considered above were observed in the experiments with ruby and Nd-glass lasers.[19,20] They are illustrated by Fig. 1. For optimal parameters of the LR lidar with the ruby laser, the spectral sensitivity to water vapor absorption coefficient at $\lambda = 694.38$ nm of the order of $\alpha_g \approx 1.4 \cdot 10^{-8}$ cm^{-1} was achieved. This is the record value for path measurements ($z = 160$ m). The results can be calibrated by means of temperature tuning of the generation band to the molecular oxygen line ($\lambda = 694.6$ nm).
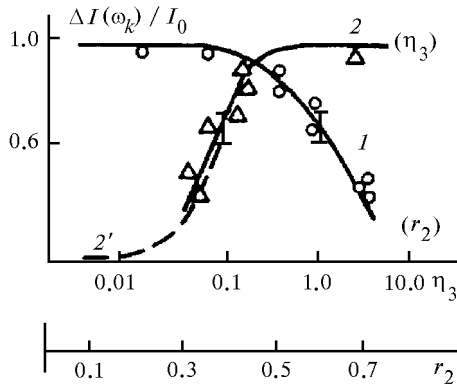

FIG. 3. Spectral sensitivity of the LR lidar with the ruby laser along 160-m path (determined from the relative depth of the gap burned out on and off the water vapor absorption line at $\lambda = 694.3$ nm) versus the reflectance of the laser output mirror r_2 at $\eta_3 = 0.1$ (curve 1) and the efficient external reflectance at $\eta_3 = 0.5$ (curve 2). Curve 2' was calculated from asymptotic formulas.

b) The case of weak echo signals characterized by asymptotic condition (7) is of primary practical interest for problems of remote gas analysis and autodyne measurements.

In this case, Godlevskii et al.[19] derived the following approximation formula for the average radiation intensity inside the laser cavity $I(\omega, z, t)$:

$$\frac{dI}{dt}\left[1 + 0\left(\frac{2z}{ct}\right) + 0\left(\frac{l}{z}\right) + 0\left(\eta_3^2\right) \right] =$$

$$= v\,\mu_0\,I\,\{k(\omega) - \beta_0 + (2l)^{-1}\ln[1 + \eta_3]\} + v\,\xi_0, \qquad (9)$$

where μ_0 is the filling of the laser cavity by the active medium; $\beta_0 = \beta_0 - \ln(r_1 r_2)/2l$; ξ_0 is the power density of spontaneous optical noise per unit of length of the cavity. Estimated relative variance in the laser radiation intensity $\delta I/I_0$ as a function of the echo signal (without absorbing gas) is

$$\delta I/I_0 \approx \eta_3\,(l\beta_0)^{-1}\,(1 + I_s/I_0),$$

where I_s/I_0 is the saturation parameter of laser pumping. When it is equal to unity, the amplification coefficient $k(\omega)$ is halved. The approximation formula for the spectral sensitivity of the LR lidar on the path with the gas absorption coefficient α_g at the frequency ω_g and uniformly broadened amplification line shape of the active medium takes the form

$$(\delta I(\omega_k) - \delta I)/I_0 \approx \eta_3\,m^2\,\alpha_g(z/l)\,\beta_0^{-1}\,(1 + I_s/I_0),$$

where $m = \gamma/\gamma_g$ is the ratio of the amplification half-linewidth to the gas absorption one.

Numerical modeling of dynamic parameters of a narrow-band laser shows that external signal leads to variation of the laser output power level δI through relaxation oscillations with characteristic frequency $\Omega_p^2 \approx (g-1)\,\beta_0\,v/t^* = 10^4 - 10^6$ Hz, where g is the excess of the laser active medium pumping over the laser generation threshold and t^* is time of spontaneous relaxation. The maximum sensitivity of the LR lidar is achieved at the instant of the build-up of the reference laser generation, when $(g - 1) \to + 0$, and the laser pumping modulation with frequencies close to Ω_p. Because of the turbulence and random character of backscattering, partially coherent echo-signal reception is generally realized on atmospheric paths (μ_n and $\mu_c \neq 0$ in Eqs. (3) and (8)).

The special case of completely incoherent reception ($\eta_3 = r_{eff} \sim z^{-2}$) can be realized in practice when the scales of spatial and temporal coherence of the fields are small compared with the aperture diameter of the receiving telescope $2R_0$ and the photon transit time along the path $2z/c$, respectively. Another special case of completely coherent reception can be realized using preliminary phase modulation of the output laser radiation by axial oscillations of a rotating mirror and subsequent synchronous detection of the amplitude of oscillating component engendered by the interference (coherent) interaction of the reference and scattered fields. For coherent reception, $\eta_3 = (2r_{eff}/r_2)^{1/2}\,\bar{B}_c$ $\sim \bar{B}_c/z$ and therefore this regime of autodyne reception is most preferable for extended paths.

In practice, because of temporal and spatial degradation of the mutual coherence of the reference and scattered fields, the potentialities of coherent reception cannot be fully realized. In particular, as for conventional (off-cavity) reception, the lidar aperture radius R_0 should not greatly exceed the spatial coherence radius of the echo-signal field ρ_c. In general, $\rho_c^{-2} = \rho_s^{-2} + \rho_0^{-2}$, where $\rho_s \approx 2z/kR_s$ is the spatial scale of coherence caused by diffuse scattering on the topographic surface illuminated with the spot of laser beam with radius R_s; $\rho_0 = b_1\sqrt{8/3}\,(1.45\,k^2\,C_n^2\,z)^{-3/5}$ is the spatial coherence radius caused by the atmospheric turbulence with the structure parameter

C_n^2; $k = 2\pi/\lambda$; b_1 is the scaling factor considering the double passage of radiation through the same inhomogeneities and the geometry of the experiment. In the specific case of external mirror reflector, the condition $\rho_c \geq R_0$ is easily met. Then we obtain $\bar{B}_c \approx 1$ for $\Omega_m > V_\perp/\rho_0$ and $\bar{B}_c \approx (0.4/\pi)\,\rho_c\,\Omega_m/V_\perp$ for $\Omega_m \ll V_\perp/\rho_0$, where Ω_m is the phase modulation frequency of output radiation, $V_\perp$ is the average atmospheric wind velocity component perpendicular to the beam axis.

FIG. 4. Sensitivity of the autodyne reception method obtained for the LR-lidar with the low-pressure CO_2 laser: a) intracavity (1) and conventional off-cavity (2) echo-signal reception at the $R(20)$ laser transition shown by circles and crosses. The solid curve is calculated at $\bar{B}_c = 0.5$; b) ratio of laser powers generated at the $R(20)$ and $P(20)$ transitions as a function of optical thickness of atmospheric absorption by water vapor ($\alpha_g z$). The transitions $R(20)$ and $P(20)$ fall on and off selective absorption lines of the H_2O molecules, respectively. Curve 1 corresponds to generation without competition (successively at the $R(20)$ and $P(20)$ transitions). Curves 2 and 3 correspond to generation with competition between the laser transitions (simultaneous generation at these transitions). Curve 2 shows the emission at $R(20)$ in

the saturated regime. Curve 3 shows the emission at the transition near the threshold of laser generation.

Figure 4 shows the sensitivity of the LR-lidar method obtained using the low-pressure CO_2 laser under laboratory conditions[22] in comparison with the sensitivity of the conventional (off-cavity) method of homodyne reception (*a*). Additional gain in the spectral sensitivity due to simultaneous measurements at two competitive transitions of CO_2 laser is also shown in the figure (*b*).

From these results it follows that autodyne reception provides more than ten-fold gain in the sensitivity of the lidar with CO_2 laser in case of one-wavelength measurements. The gain is increased by a factor of 10 in case of competition between the coupled laser transitions. The last result was also verified in the experiments[29] performed at the IAO SB RAS with a He-Ne laser operating simultaneously at 0.63 and 3.39 μm. Absolute sensitivity for the above type of autodyne CO_2 laser[26] was as high as $4 \cdot 10^{-17}$ W/Hz. It can be increased with the increase of pumping stability and temporal coherence of the reference laser, incorporation of the autodyne reception scheme into conventional electronic scheme of balance measurements, and use of off-axis optics in the transceiving reflecting telescope. Principal possibility of using oncoming competitive laser beams, for instance, in an annular laser (laser gyroscope) and bistatic sounding scheme with a powerful laser transmitter and a low-noise autodyne laser operating near its generation threshold,[1,5] which has not yet been checked experimentally, also should be mentioned. In this connection, the use of a hybrid laser in the schemes of laser reception of echo-signals seems to be promising.[26]
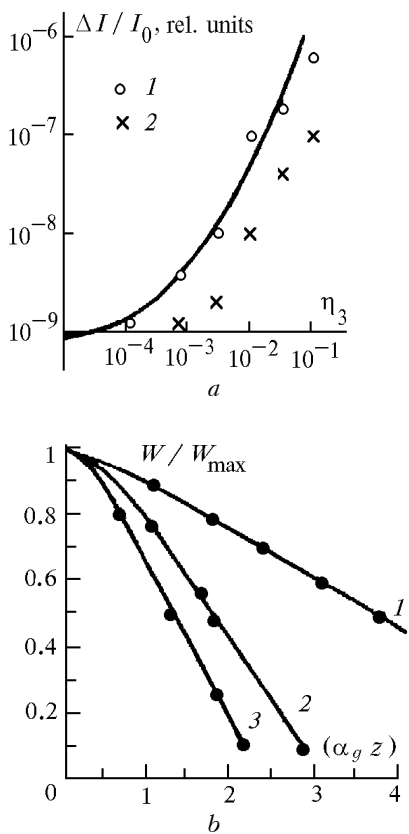
2.2. LR−lidar models for supersensitive gas analysis

A number of LR-lidar models for atmospheric gas analysis that implement the idea of autodyne reception were first developed and tested at the IAO SB RAS. Laser sources on Ar, He-Ne, CO_2, and the above-mentioned ruby and Nd-glass lasers were used.[19–22]

Transitions at 496.5 and 515.5 nm were chosen as working for the 1-W cw Ar^+-ion laser of the LR lidar. These laser lines fall on the center and wing of the NO_2 absorption line in the atmosphere. Modulation technique of autodyne reception at operating frequency $\Omega_m = 1$ kHz was used. The sensitivity to the NO_2 concentration of about 0.05 ppb was achieved on 160 m path. The laser autodyne simultaneously operates as an optical filter with the bandwidth $\Delta\Omega \approx 0.001$ cm^{-1}.

A pilot model of multipurpose LR lidar with low-pressure tunable CO_2 laser was developed in the Laboratory of Nonlinear Optical Diagnostics.[5,22] At present, this model is successively used at the IAO SB RAS for experimental investigation of novel modifications of the autodyne measurement method.[26]

The laser can be discretely tuned by controllable mirrors based on piezoceramic plates to 70 transitions of $P-$ and $R-$ branches as well as to sequent bands thereby providing tuning to the lines of selective absorption of more than 30 gases and vapors such as NH_3, CH_4, C_2H_6, O_3, CO_2, NO_2, H_2O, and so on.

An example of path measurements of diurnal variations of concentrations of some atmospheric pollutants[1] using the LR lidar with the CO_2 laser is shown in Fig. 5.
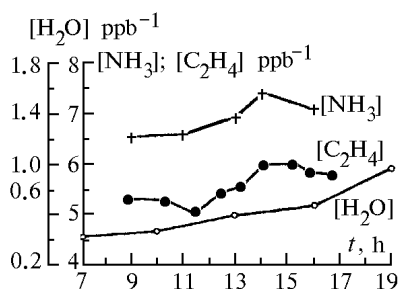

FIG. 5. Example of path gas analysis with the LR lidar on the basis of the CO_2 laser tunable to transitions of $P-$ and $R-$ branches. Diurnal behavior of concentrations of C_2H_4, NH_3, and H_2O in the atmosphere in the vicinity of an industrial center was measured on 500-m path.

The obtained experimental results demonstrate the potentialities of the autodyne echo-signal reception with CO_2 laser to solve such problems as monitoring of the atmospheric turbulence,[22] bathymetry[30,31] detection and ranging of dynamic characteristics of objects,[1,26] and acoustic-optical detection.[28] Let us consider the last effect more closely.

2.3. Laser autodyne acoustic antennas

Principal possibility of developing extended (field) antenna systems of a novel type for recording of acoustic radiation power in the atmosphere and establishing the position of a sound source based on acoustic-optical interaction in atmospheric sections of laser resonators was demonstrated in Ref. 28. When the laser pumping parameter $(g-1) \to +0$, acoustic modulation of the $Q-$ factor of the external atmospheric section of the laser resonator with strong feedback satisfying conditions (5) and (6), engenders modulation of the detected laser radiation of the autodyne. The external signal parameter η_3, specified by Eq. (8), must consider the phase run-on of the optical wave along the beam axis caused by acoustic perturbation of the medium. Our analysis demonstrates that in case of the acoustic wave, propagating perpendicular to the laser beam axis, the maximum acoustic-optical intracavity interaction occurs when the laser beam radius is equal to the acoustic radiation wavelength. When the direction of the acoustic wave propagation deviates from perpendicular, the

interaction is maximum if the odd number of acoustic half-waves falls on the atmospheric section of the resonator of length z. Figure 6 shows the results of acoustic-optical measurements[28] using the autodyne lidar with the CO_2 laser. The effect of autodyne acoustic-optical interaction established experimentally calls for further theoretical and experimental investigations.
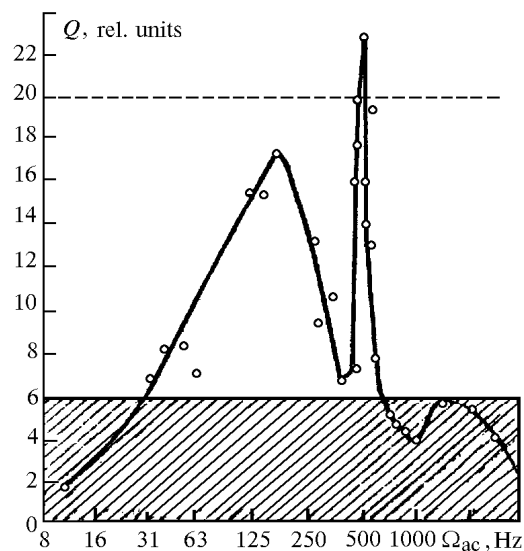

FIG. 6. Acoustic radiation spectrum $Q(\Omega_{ac})$ of the atmospheric source recorded by the laser autodyne with an external mirror reflector. The solid curve approximates experimental points. The hatched area indicates the level of the intrinsic noise.

2.4. Laser autodyne detection of capillary waves and adsorbed states at an interface

The high sensitivity of laser autodyne to external signal amplitude and phase has been established by the author for remote detection of small-amplitude and high-frequency oscillations of the sea surface[30] (capillary and sound waves). The capillary waves are important indicators of various oceanic processes (internal waves) and sleek and films of surface-active substances as well. In addition, the idea of developing continuous information channel for communication between the ocean and the atmosphere using an underwater sound source and remote laser sounding of the interface from an atmospheric platform seems to be very attractive.

A series of experiments aimed at finding the threshold sensitivity of the autodyne laser wave detector ($\lambda = 10.6$ μm) to the sea surface roughness was performed in a water reservoir using a calibrated source of capillary waves.[30] Instability of the laser frequency was 10^{-11}. Figure 7a shows the measured level of demodulated autodyne signal ($\Omega_m = 220$ Hz) versus the capillary wave amplitude. The signal is maximum when

the amplitude of the capillary waves approaches the quarter of the CO_2-laser wavelength. The threshold sensitivity was determined by the electric noise of the photodetector and was as high as $\lambda/10$. The voltage sensitivity was $\sim 10^4$ V/cm. The energy spectra of capillary waves in the frequency range 200–2500 Hz were obtained within the zone of sea surf. The spectra peaked at 25, 10^2, and $(0.6–2.5) \cdot 10^3$ Hz. The feasibility of remote detection of high-frequency spectra of water surface from the IL-14 aircraft-laboratory (flight altitude $z = 710–800$ m, speed $V_\perp = 190$ km/h) was demonstrated in the experiments[31] performed at the IAO SB RAS using the autodyne lidar with the cw CO_2 laser with an output power of ~ 2.7 W and a receiving telescope 160 mm in diameter. The FSG-22A cooled photodetector was used for intracavity reception.
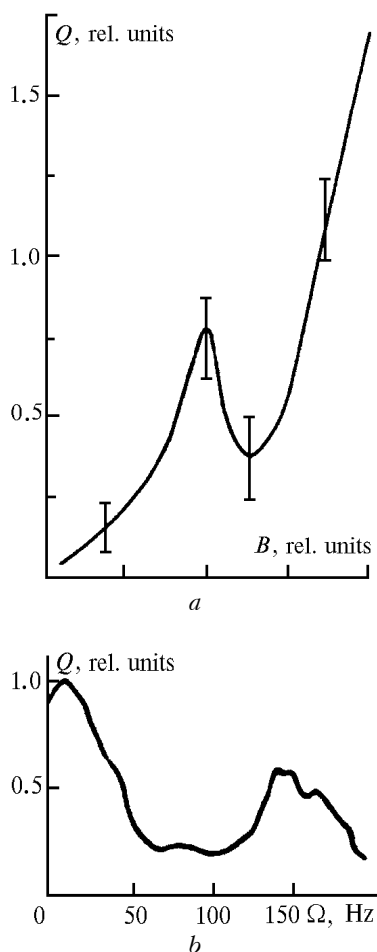

a

b

FIG. 7. Laboratory (a) and airborne (b) experiments on detection of the high-frequency component of sea surface roughness using the laser autodyne with the CO_2 laser. The sensitivity of coherent autodyne lidar Q to microcapillary wave amplitude B at modulation frequency $\Omega_m = 220$ (a); the example of energy spectrum of sea surface roughness measured by scanning with the lidar field of view with a linear speed of 190 km/h (b).

An example of reconstruction of the energy spectrum of reflected signal fluctuations is presented in Fig. 7b.

Thus, the method and means for laser autodyne measurements provide supersensitive detection of not only the spectra of low-frequency energy-carrying waves, but also the most informative capillary component of sea surface roughness in the frequency range 10–10000 Hz.

In conclusion, the method of intracavity adsorption (autodyne) spectroscopy of surface-active substances, adsorbed gases, and aerosols should be mentioned. It was suggested at the Laboratory headed by the author.[32] In that paper, substantially nonlinear response of the ruby laser to adsorption and desorption of molecules on the optical elements of the cavity was found experimentally.

The zones of disturbance of total internal reflection can be used as external sections of the laser autodyne resonator, in particular, extended light guides can be used for sensing of molecules of substances adsorbed on the light guide surface.

I would like to acknowledge Academician V.E. Zuev for his support of this work and creative participation in the problem development.

REFERENCES

1. V.E. Zuev, A.A. Zemlyanov, and Yu.D. Kopytin, *Nonlinear Atmospheric Optics* (Gidrometeoizdat, Leningrad, 1989), 256 pp.

2. A.P. Godlevskii and Yu.D. Kopytin, Zh. Prikl. Spectr. **31**, No. 4, 240–247 (1979).

3. A.P. Godlevskii, Yu.D. Kopytin, V.A. Korol'kov, and Yu.V. Ivanov, Zh. Prikl. Spektr. **39**, 734–740 (1983).

4. V.E. Zuev, ed., *Sensing of Physical-Chemical Parameters of the Atmosphere Using High-Power Lasers* (Publishing House of the IAO SB AS USSR, Tomsk, 1979), 220 pp.

5. I.V. Samokhvalov, Yu.D. Kopytin, I.I. Ippolitov, et al., *Laser Sensing of the Troposphere and Underlying Surface* (Nauka, Novosibirsk, 1987), 261 pp.

6. H. Moenke and L. Moenke, *Einfuhrung in die Laser Micro-Emissonspectral Analyse* (Akademische Verlagsgesellschaft Geest & Portig K.G., Leipzig, 1966), 250 pp.

7. E.B. Belyaev, Yu.D. Kopytin, S.T. Penin, and S.A. Shishigin, Atmos. Oceanic Opt. **7**, No. 5, 353–354 (1994).

8. S.S. Bessarab, S.T. Penin, V.A. Chikurov, and L.K. Chistyakova, Atmos. Oceanic Opt. **9**, No. 1, 44–46 (1996).

9. V.E. Zuev, A.A. Zemlyanov, Yu.D. Kopytin, and A.V. Kuzikovskii, *High-Power Laser Radiation in the Atmospheric Aerosol* (Nauka, Novosibirsk, 1984), 223 pp.

10. Yu.V. Akhtyrchenko, E.B. Belyaev, Yu.V. Vysotskii, et al., Izv. Vyssh. Uchebn. Zaved. SSSR, Ser. Fizika **26**, No. 2, 5–13 (1983).

11. V.E. Zuev, Yu.D. Kopytin, and A.V. Kuzikovskii, *Nonlinear Optical Effects in Aerosols* (Nauka, Novosibirsk, 1980), 180 pp.

12. D.A. Cremers and L.J. Radziemski, Appl. Spectrosc. **39**, 57−65 (1985).

13. L.J. Radziemski, D.A. Cremers, and T.R. Loree, Spectrochem. Acta **38B**, 347−355 (1983).

14. L.J. Radziemski, R.W. Solarz, and J.A. Paisner, eds., *Laser Spectroscopy and its Application* (Marsel Dekker Inc., New York, 1987).

15. Yu.V. Akhtyrchenko, et al., in: *Abstracts of Reports at the Eigthts All-Union Symposium on Laser and Acoustic Sounding of the Atmosphere*, Tomsk (1984), Vol. 2, pp. 114−118.

16. E.B. Belyaev, Yu.D. Kopytin, A.P. Godlevskii, et al., Pis'ma Zh. Tekh. Fiz. **8**, No. 6, 74−80 (1982).

17. L.G. Shamanaeva, Yu.D. Kopytin, and N.P. Krasnenko, "*Method for determining of the aerosol particle number density in the atmosphere*,B Inventor's Certificate No. 1028174.

18. L.G. Shamanaeva, Yu.D. Kopytin, and N.P. Krasnenko, in: *Abstracts of Reports at the Seventh All-Union Symposium on Laser and Acoustic Sounding of the Atmosphere*, Tomsk (1982), Vol. 2, pp. 126−130.

19. A.P. Godlevskii, V.E. Zuev, A.K. Ivanov, and Yu.D. Kopytin, Dokl. Akad. Nauk SSSR **267**, No. 2, 343−347 (1982).

20. A.P. Godlevskii and Yu.D. Kopytin, Kvant. Elektr. **9**, No. 9, 2007−2012 (1982).

21. V.E. Zuev and Yu.D. Kopytin, Izv. Akad. Nauk SSSR, Ser. Fiz. **49**, No. 3, 418−427 (1985).

22. A.P. Godlevskii, Yu.D. Kopytin, and S.V. Lazarev, Kvant. Elektr. **13**, No. 5, 1259−1263 (1986).

23. T.P. Belikova, E.A. Sviridenkov, and A.F. Suchkov, Usp. Fiz. Nauk **113**, No. 2, 327−329 (1974).

24. S.F. Luk'yanenko, M.M. Makogon, and L.N. Sinitsa, *Intracavity Laser Spectroscopy. Principles and Applications* (Nauka, Novosibirsk, 1985), 120 pp.

25. R. Loudon, M. Harris, T.J. Shepherd, and J.M. Vaughan, Phys. Rev. **A48**, 681 (1993).

26. E. P. Gordov, Atmos. Oceanic Opt. **8**, Nos. 1−2, 137−144 (1995).

27. *Abstracts of the First Workshop on Optical Amplifiers for Lidar Applications*, OSA (1991), Vol. 12; *Technical Digest on Coherent Laser Radar Technology and Applications*, OSA (1991), Vol. 12; *Proc. of the Seventh Conference on Coherent Laser Radar Applications and Technology*, France (1993).

28. Yu.D. Kopytin and L.G. Shamanaeva, in: *Abstracts of Reports at the First Interrepublic Symposium on Atmospheric and Oceanic Optics*, Tomsk (1994), Vol. 2, p. 157; Izv. Vyssh. Uchebn. Zaved. SSSR, ser. Fizika (VINITI, Moscow,1996), No. 92−D96, 1996).

29. A.I. Zhiliba and P.N. Sharin, Atm. Opt. **4**, No. 2, 183−185 (1991).

30. S.F. Balandin, I.A. Zinkin, Yu.D. Kopytin, et al., Opt. Atm. **1**, No. 6, 150−154 (1988).

31. S.D. Burakov, A.P. Godlevskii, and S.A. Ostanin, Atm. Opt. **3**, No. 5, 498−502 (1990).

32. A.P. Godlevskii and Yu.D. Kopytin, Zh. Prikl. Spektr. **29**, No. 5, 791−795 (1978); *Abstracts of Reports at the Fourth All-Union Symposium on Propagation of Laser Radiation in the Atmosphere*, Tomsk (1977), Vol. 1, p. 44.

33. S.F. Balandin, Yu.D. Kopytin, V.M. Klimkin, et al., Atmos. Oceanic Opt. **9**, No. 1, 64−66 (1996).